

Thermal Analysis and Macrostructure of Fe-Si Alloys

M. G. González-Flores*, J. A. García-Hinojosa

Department of Metallurgical Engineering-Faculty of Chemistry, National Autonomous University of Mexico, UNAM,
Coyoacán, Ciudad de México, México

ABSTRACT

The high electrical and magnetic properties that possess Fe-Si alloys makes them useful materials in the electricity sector as well as in new technological and energy applications. The effect of silicon addition in non-equilibrium transformations of Fe-Si alloys was analyzed via cooling curves analysis, macrostructural characterization and hardness profiles. Two alloys Fe-Si with commercial level impurities were produced by melting. The thermal history was recorded and analyzed throughout the solidification and cooling ranges for each alloy. Samples were sectioned for their characterization and then, resistance to plastic deformation was quantified through a hardness test. Results show that, small increases in the percentage of silicon alter the final morphology because to the presence of more transformations during cooling of samples caused by expansion of the gamma region.

Keywords: Electrical Steels, Macrostructure, Cooling Curve Analysis, As-Cast, Columnar-Equiaxed Transition

I. INTRODUCTION

Fe-Si alloys are materials with high electrical and magnetic properties. These features allow and make possible use them at industrial scale in the construction of electric motors, transformers and new applications such as wind generators and electric cars [1, 4-7, 10].

At present, the main way of making not oriented silicon steel sheets is by continuous casting processes followed by hot and cold rolling. These procedures allow decrease waiting time and manufacturing cost as well as increased the product quality and their repeatability. This methodology, however, have some drawbacks with increasing silicon concentration. The increase in hardness and brittleness of the material make difficult subsequent processing. At the same time, morphological variations of the structure (shape and size) and segregation problems in these materials are frequent. [2, 6-10].

Alternative methods for making thin sheets such as Chemical Deposition Vapor (CVD) of silicon and melt spinning have been reported. While these methods allow the production of alloys with high percentages of silicon, their use is restricted in commercial scale because is still

inappropriate. Several studies carried out have focused on improving properties by improving the texturing process. The great difficulty, in many cases, is the structural heterogeneity in these steels. It has been observed that the initial structure significantly affects the evolution of texture and consequently, the magnetic properties of the final product. Samples with grain sizes and shapes not similar initially, will record significantly different textures in different stages of annealing and cold rolling [9-13, 17].

Otherwise, the evolution of grain size and shape under casting conditions has received trifling attention. This is contradictory because of the electrical and magnetic properties are not only derived from the chemical composition of the alloy. These properties strongly depend on the solidification structure achieved under processing conditions.

Therefore, a study focused on the characterization of the casting structure as well as a quantification of hardness is important because its knowledge is essential in the electrical steels manufacturing. The above is relevant because it allows relate the initial morphology with the texture evolution and consequently with the final properties of the material. This research studies the

thermal history, the cast structure and hardness pattern of two alloys Fe-2.5 wt. % Si and Fe-3 wt. % Si by thermal analysis cooling curves, microstructural characterization of the ingot and hardness measurement of punctual form.

II. METHODS AND MATERIAL

A. Manufacture of the experimental alloys and thermal analysis

Two alloys Fe-Si with commercial level impurities were prepared by melting in an induction furnace coreless with a capacity of 20 kg. A controlled chamber atmosphere of Argon gas was used. The liquid metal was poured in a permanent mold to obtain ingots with the following dimensions: length= 5 cm, width= 15 cm, and height= 35 cm (Figure 1).

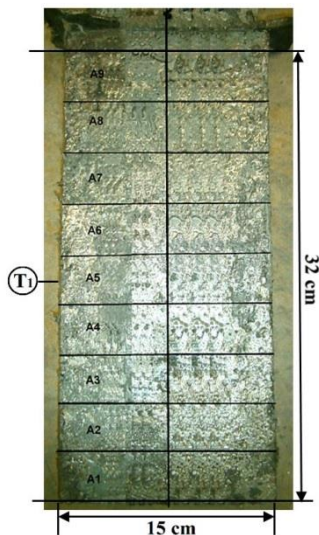


Figure 1. Experimental sample casting (ingot)

Thermal history of each alloy was recorded through two type B thermocouples introduced in the center and other one on the periphery of the mold in the central region (T1, Figure 1 and 2). The accuracy of the readings was ± 2.5 ° C. The record in temperature variation versus time was carried out with an Iotech data acquisition Tempscan[®] 1100 connected to a personal computer. In order to reveal the exact temperatures at which the main phase changes occur, the cooling rate versus time was used. Calculation of pseudobinary and pseudoternary phase diagrams were performed by the Thermo-Calc program in the area of interest and used for validate the

changes. Both experimental and calculated values were compared with those reported in the literature [14-16].

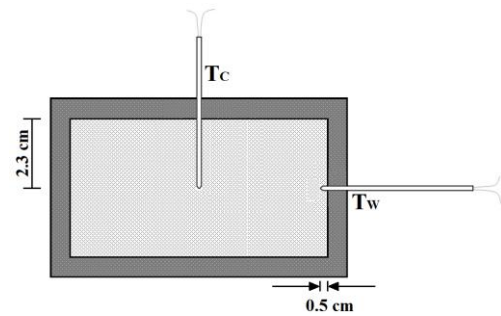


Figure 2. Schematic representation of thermocouples distribution in the ingot

B. Macrostructural Analysis

Macrostructural evaluation of the ingots was carried out. Samples were sectioned to characterize the structure completely. A court longitudinal in the central region of the ingot was realized; thereupon each sample was cut again at nine sections. Three representative samples of each ingot were selected: top= A9, middle= A5 and bottom= A1, as seen in figure 1. Samples in their casting condition were prepared for characterization structural by standard metallographic procedures. Finally, these were attacked with a fresh mixture of acids with composition: 1:1 HNO₃ and CH₃-COOH.

C. Hardness Profiles

Resistance to plastic deformation was quantified in both alloys through a hardness test. Hardness Rockwell A measurements on the selected parts of each alloy (A1, A5 and A9) were carried out. Measurements were made from mold wall (0.2 mm) to the center of the workpiece with a spacing of 3 mm between readings.

III. RESULT AND DISCUSSION

A. Chemical Composition

The chemical compositions were obtained by atomic absorption spectrophotometry. Table 1 shows weight percent of the major alloying elements in the two alloys under study.

Table 1. Chemical composition of the experimental alloys Fe-Si

Chemical Composition (w/w)											
Alloy	Si	C	Mn	Cr	Mo	Ni	Al	Cu	P	Others	Fe
1	2.54	0.02	0.54	0.06	0.04	0.02	0.02	0.15	0.01	0.08	96.50
2	3.10	0.03	0.57	0.04	0.04	0.02	0.01	0.03	0.01	0.02	96.10

B. Thermal Analysis

The thermal evolution for both alloys considering a binary system predicts the formation of a single phase, i.e., solidification and cooling of the alpha phase without passing through the gamma loop [16]. However, the presence of more components causes a modification of the transformation lines. Cooling curves recorded the main transformations identified by equilibrium phase diagrams during cooling [14-16]. Similar values for liquidus and solidus were obtained with the computer program Thermo-Calc. The thermal history of each alloy is shown below. In figure 3a) the cooling curve of the Fe-2.5 wt. % Si alloy and its derivative are observed. When the solidification of the sample starts, the latent heat involved slows the cooling rate of the alloy. Exothermic peaks 1 and 2 indicate the start and end the formation of the α phase, respectively.

The recorded values are slightly higher than the reported amounts [11-13] and the calculated by Thermo-Calc. The peritectic transformation of a fraction of the (α) phase to ($\alpha + \gamma$) phase in the presence of low concentrations of C, Mn, Cu and Ni is indicated with peak 3. Ferrite stabilized due to the action of silicon is observed in the biphasic first interval of both alloys. The peritectic transformation gives rise to a second stage in the transformation process, i.e., the formation of the gamma phase from the peritectic reaction. The reported value indicates an increase in peritectic transformation temperature (A4 line). Alternatively, the exothermic peak 4 marks the beginning of the gamma loop while the peak 5 indicates the end of the biphasic region $\alpha + \gamma$. The addition of stabilizers alters the extension of gamma region in diagram Fe-Si. In this situation, a sequence of phase transformations more complex with a content B smaller due to the emergence of more polymorphic transitions are presented.

The maximum aperture of the gamma loop (zone $\alpha + \gamma$) reaches only 2.5 wt % Si for the binary case and extends up to 3.5 wt % Si for the ternary case (Fe-Si-C).

Additional transformations are recorded in the cooling curve of the alloy. The possible formation of SiC, and $Mn_{11}Si_{19}$ MnSi compounds are indicated with the peaks 6, 7 and 8, respectively.

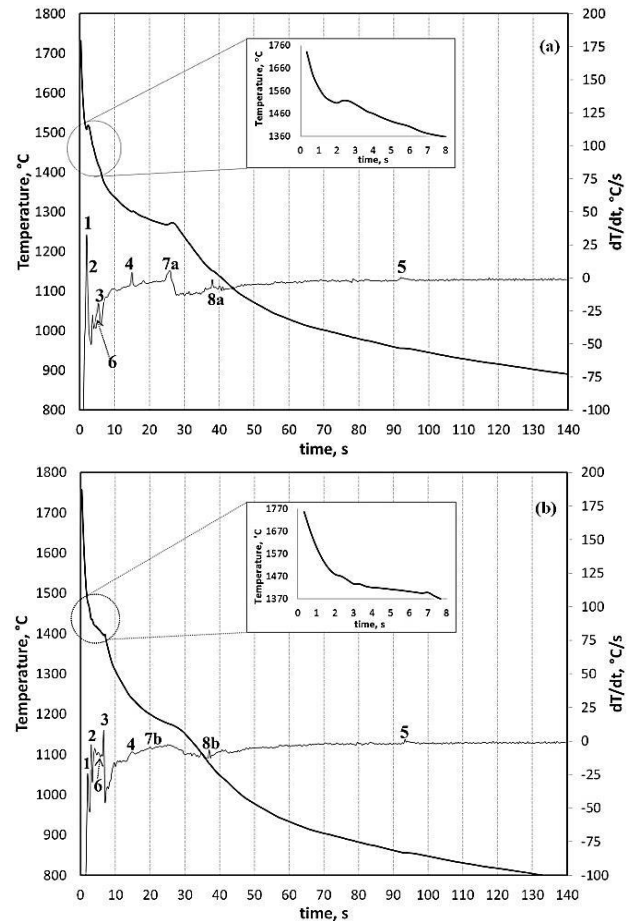


Figure 3. Thermal analysis, temperature and events:
 (1) Liquidus temperature (T_L). Start of growth of primary phase $L \rightarrow L + \alpha(\delta)$
 (2) Solidus temperature (T_S). End of solidification $L + \alpha(\delta) \rightarrow \alpha(\delta)$
 (3) Peritectic transformation $\alpha(\delta) \rightarrow \alpha(\delta) + \gamma$
 (4) Gamma loop start $\alpha(\delta) + \gamma \rightarrow \alpha + \gamma$
 (5) Gamma loop finish $\alpha + \gamma \rightarrow \alpha$
 (6) Formation of SiC
 (7a) Formation of MnSi, (7b) Formation of $\alpha Fe, \beta Fe_2Si$
 (8a) Formation of $Mn_{11}Si_{19}$, (8b) Formation of Mn_3Si

Similar transformations during solidification and cooling are observed in the alloy 2. Figure 3b) shows the cooling curve and the cooling rate of the alloy.

Table 2. Phase transformation temperatures for the experimental alloys Fe-Si.

Transition Temperature	Transformation sequence	Alloy 1		Alloy 2	
		Reported ^{11,12}	Measured	Reported ^{11,12}	Measured
T _L (°C)	$L \rightarrow L + \alpha$	1495 [*] , 1494	1507	1488 [*] , 1485	1479
T _S (°C)	$L + \alpha \rightarrow \alpha$	1465 [*] , 1466	1475	1453 [*] , 1457	1454
Solidification range		30 [*] , 28	32	35 [*] , 28	25
Peritectic transformation	$\alpha(\delta) \rightarrow \alpha + \gamma$	1394	1398	1394	1395
Gamma loop start	$\alpha + \alpha(\delta) + \gamma \rightarrow \alpha + \gamma$	1282	1300	1244	1240
Gamma loop finish	$\alpha + \gamma \rightarrow \alpha$	890	955	840	855
Gamma loop range		392	345	404	385
Others					
SiC		1414	1416	1414	1413
MnSi		1269.6	1269		
Mn ₃ Si ₂		1150.2	1151		
$\alpha Fe, \beta Fe_2 Si$				1200	1199.5
Mn ₃ Si				1075	1077

* These data were obtained using Thermo-Calc

The first three peaks of exothermic nature represent the transformations due to the crossing of the liquidus (1) and solidus (2) lines as well as the peritectic transformation (3). Subsequent to this ultimate transformation occurs a drop in the cooling rate of the material. The begin and end of the biphasic region ($\alpha + \gamma$) given by the gamma loop are indicated by peaks 4 and 5, respectively. Finally, the peak 6 represents one more time the formation of compound SiC, while 7b and 8b indicate the formation of $\alpha Fe, \beta Fe_2 Si$ and Mn₃Si, respectively. While the extension of the gamma region increases with the percentage of carbon for a fixed value of silicon, the data obtained are lower than those reported for both alloys. The presence of Mn, Cu and Ni prevent increasing of gamma loop for a composition given and reduce their extension in a temperature range. It is well known that the lower the solidification interval (SI), the sample tends to form a columnar grain area as well as a small chill zone with fine equiaxed grain (short solidification range). The alloy 2 has a lower solidification interval compared with alloy 1. Therefore, one would expect to observe a predominantly columnar structure in the first case while in the second one, a slightly more equiaxed region for a binary case. However, due to the presence of C, Mn, Cu and Ni the transition lines experience a lag so that the final morphology is modified causing a columnar zone lesser for the alloy with a smaller solidification range. A summary of the changes mentioned are shown in Table 2. All temperatures given in the table are the average values of three measurements carried out for each alloy.

C. Macrostructural Analysis

Macrostructures of ingots with different content of silicon are shown in Figure 4. In general, the samples analyzed exhibiting the macrostructure characteristic of a material that solidifies under a solidification pattern intermediate. The presence of columnar grains on the edge of the piece and their subsequent transition to equiaxed grains as they approached to the center of the ingot, were observed. The columnar-equiaxed transition (CET) is evident in all samples but is more pronounced in the alloy 2 which shows a finer morphology. Macro and micro-shrinkages scattered along the ingot are observed in the two alloys under study.

Summary of the structural characteristics of both alloys is shown in table 3. Small increases in both Silicon and Carbon produce a change in the temperatures distribution. As a consequence, the morphological transition is presented at a shorter distance. The distance between the CET position and the ingot surface is shown in figure 5. The distance of the CET in the upper region of ingot is similar for both materials while for the alloy 1 there is not significant variation. This suggests that the critical condition of the CET is satisfied in entire length of the ingot for the alloy 1.

Table 3. Macrostructural characteristics of the samples

Alloy	Macrostructural Solidification Pattern		Position	Columnar zone (%)	Equiaxed zone (%)	CET distance from the mold wall (cm)	Ratio LW (mm/mm)	
	Theoretical	Experimental					CZ	EZ
1	Long (equiaxed grains)	Mixed (Equiaxed-Columnar)	Top	87.04	12.96	1.148	9.47	1.13
			Middle	87.04	12.96	1.148	9.42	1.07
			Bottom	83.23	16.77	1.092	7.64	1.07
2	Long (equiaxed grains)	Mixed (Equiaxed-Columnar)	Top	83.23	16.77	1.092	7.43	0.99
			Middle	73.23	26.77	0.924	10.24	0.92
			Bottom	59.60	40.40	0.7	7.12	0.92

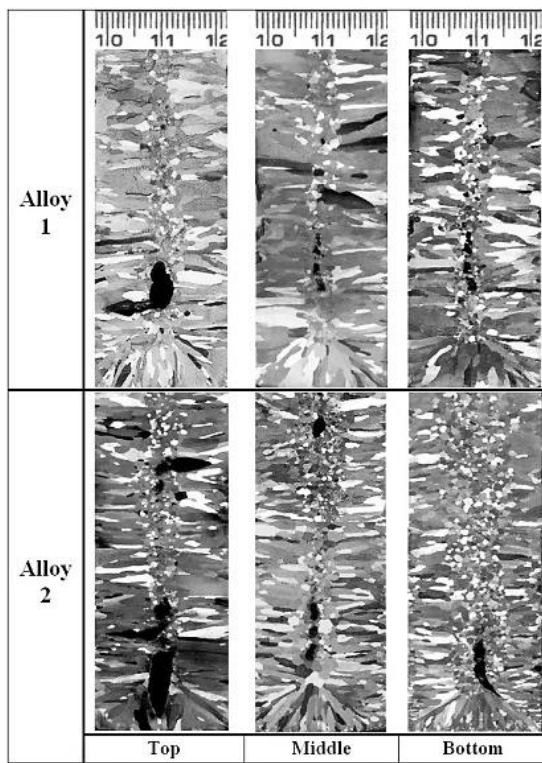


Figure 4. Macrostructure of electrical steels

Considering both materials, this condition is satisfied only in the upper region of the ingot. Alloy 1 shows a columnar structure at the basis of the ingot equivalent to 83% of the area analysed. In the surface thereof, a 87% of columnar structure is obtained. Considerable variation along the casting is not observed, the structure is homogeneous and the distance of the transition is similar in the three regions analyzed. Furthermore, alloy 2 has a greater morphological variation. The columnar zone changes depending of the piece length increasing from 60% at the base of the ingot up to 83% in the upper region thereof so that the distance of the CET passes 0.7 cm at the base of the ingot to 1.09 cm on the surface thereof (figure 5). The increase in the equiaxed zone may be due to the effect of impurities in the melt. This is possible also, due to forced nucleation generated during the poured through the initial cooling action of the mold and then to be transferred to the interior of melt. If the nucleation of equiaxed grains occurs these will have favorable conditions and grow up ahead of the columnar interface.

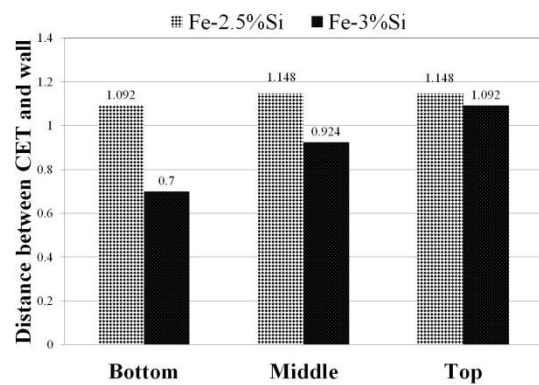


Figure 5. Distance between CET and mold wall

Similarly, an increase in the undercooling on the liquidus region causes that the columnar-equiaxed transition is presented at a shorter distance. The results indicate that this relationship does not hold for this alloy system. Alloy 1 has a slightly higher undercooling. However, thermal and solute variations are greater with the increase in concentration as occurs in alloy 2. The formation of the central equiaxed zone is also favored by the abrupt change in the crystalline arrangement across the gamma loop for the case of alloy 2.

The final size of ferrite grains for both alloys already without phase transformation is a limiting step. Even though is required of a lower activation energy this one is a very slow growth process due to the high "activation energy barrier." This phenomenon is because that to the difference in chemical composition leads to different mechanisms of movement of grain boundaries. The higher percentage of alloying elements, the greater phases difference formed at elevated temperatures. The existence of a second phase due to the austenite loop, acts as an inhibitor for the growth of ferritic grains. Thus, the elements in solid solution enrich preferentially the grain boundary in motion and reduce the mobility due to the drag effect of solute.

D. Hardness profiles

The results of tests Rockwell A hardness performed are shown in Figure 7.

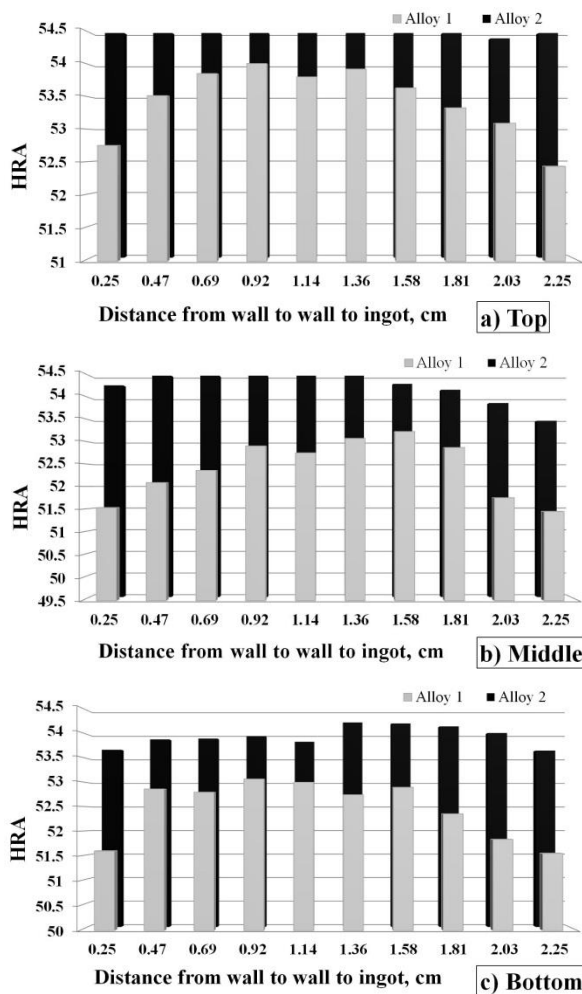


Figure 6. Effect of Silicon content and position of the samples on the Hardness property

Significant differences are observed from wall to wall for alloy 1. The CET causes considerable variation in the hardness values. Maximum values are obtained in the center of the piece, which corresponding to the equiaxed zone. The predominantly columnar region recorded the lowest hardness values. The same behavior was observed in all three regions analyzed (top, middle and bottom, figure 6). Alloy 2 by not submitting a CET with such a marked change does not show the same behavior. Considerable variations throughout the sample are not observed as in the case of Alloy 1 (7a and 7b). Alternatively, are presented changes similar to the alloy 1 at the bottom of the ingot. The inhomogeneity in the size and shape of the grains led to variations in the hardness values in this section such as presented for alloy 1. The distortion in the material is increased because of the sudden pass by the bi-phase region ($\alpha+\gamma$) which causes an increase in the hardness value of the alloy 2.

IV. CONCLUSION

Thermal analysis together with macrostructural characterization and hardness profiles permit to study the effect of silicon in the Fe-Si system as a function of composition. The results showed that small increases in the percentage of silicon alter the morphology of the samples. As the percentage of silicon increased the columnar-equiaxed transition is occurred at a shorter distance. The presence of elements such as C, Mn, Cu and Ni extend and expand the gamma region generating more transformations during cooling of samples. The increase and maintenance of the hardness values were due to the rapid crossing by the gamma area.

V. ACKNOWLEDGEMENT

The authors acknowledge the financial support from Consejo Nacional de Ciencia y Tecnología (CONACYT). We also thank to A. Gerardo Ruiz-Tamayo for the technical support.

VI. REFERENCES

- [1] V. A. Aranda, J. A. García. 2012. Study of the Macroseggregation of Silicon in Steels for Electrical Applications. MRS Proceedings, Advanced Structural Materials, 2012, Vol. 1373. ISSN 1946-4274, DOI: 10.1557/opl.2012.299.
- [2] J. A. García, M. H. Cruz. 2012. Effect of Silicon on the Cast Macrostructure of Fe-Si alloys. MRS Proceedings, Structural and Chemical Characterization of Metal Alloys and Compounds, Vol. 1372. ISSN 1946-4274, DOI:10.1557/opl.2012.127.
- [3] M. G. González, J. A. García. 2012. Microstructural study of as-cast Fe-Si alloys. MRS Proceedings, Structural and Chemical Characterization of Metal Alloys and Compounds, Vol. 1372. ISSN 1946-4274, DOI:10.1557/opl.2012.130.
- [4] J. Barros, T. Ros-Yañez. 2005. The effect of Si and Al concentration gradients on the mechanical and magnetic properties of electrical steel. Journal of Magnetism and Magnetic Materials, April 2005, Vol. 290-291, Part 2. ISSN NO: 0304-8853 DOI:10.1016/j.jmmm.2004.11.547.

- [5] J. Barros, Y. Houbaert. 2005. Modeling Silicon and Aluminum Diffusion in Electrical Steel. *Journal of Phase Equilibria and Diffusion*, July 2005, Vol. 26, No. 5. ISSN NO: 1547-7037, DOI: 10.1361/154770305X66457.
- [6] S. Nakashima, K. Takachima. 1997. Effect of Silicon content and carbon addition on primary recrystallization of Fe-3 pct Si. *Metallurgical and Materials Transactions*, March 1997, Vol. 28, Issue 3. ISSN: 1073-5623, DOI: 10.1007/s11661-997-0054-1.
- [7] F. Kováč, M. Dzubinský. 2004. Columnar grain growth in non-oriented electrical steels. *Journal of Magnetism and Magnetic Material*, 2004, Vol. 269, ISSN NO: 0304-8853, DOI: 10.1016/S0304-8853(03)00628-0.
- [8] J.T. Park, J. A. Szpunar. 2009. Effect of initial grain size on texture evolution and magnetic properties in nonoriented electrical steels. *Journal of Magnetism and Magnetic Material*, 2009, Vol. 321, ISSN NO: 0304-8853, DOI:10.1013/j.jmmm.2008.12.015.
- [9] Y. Sidor, F. Kovac. Microstructural aspects of grain growth kinetics in non-oriented electrical steels. *Material Characterization*, January 2005, Vol. 55. ISSN: 0026-0673, DOI: 10.1016/j.matchar.2005.01.015.
- [10] F. J. Landgraf, T. Yonamine. 2003. Magnetic properties of Silicon Steel with as-cast columnar structure. *Journal of Magnetism and Magnetic Material*, January 2003, Vol. 254-255. ISSN NO: 0304-8853, DOI: 10.1016/S0304-8853(02)00869-7.
- [11] A. I. Yatsenko, P.D. Grushko. 1993. The primary structure of Silicon Steels. *Metal Science and Heat Treatment*, February 1993, Vol. 35, Issue 2. ISSN: 0026-0673, DOI: 10.1007/BF00773796.
- [12] H. Liu, Z. Liu. 2011. Solidification structure and crystallographic texture of strip casting 3 wt.% Si non-oriented silicon steel. *Materials Characterization*, February 2011, Vol. 62. ISSN: 0026-0673, DOI:10.1016/j.matchar.2011.02.010.
- [13] Z. Ning, Y. Ping. 2012. Influence of columnar grains on the recrystallization texture evolution in Fe-3%Si electrical steels. *Acta Metallurgica Sinica*, Vol. 48, Issue 3. DOI: 10.3724/SP.J.1037.2011.00699.
- [14] Landolt-Börnstein. Ternary alloy systems. Material Science and International Team, MSIT, Springer, 2008, Vol. 11, subvolume D, part 2. Heidelberg 2008, Germany. ISBN 978-3-540-69759-6.
- [15] Y.Luo. 1988. Partial Phase Diagram of Fe-Si (≤ 8 mass% Si)-C(≤ 0.8 mass% Si) and Pseudobinary Sections of Fe-Si and Fe-C. *Acta Metallurgica Sinica*, June 1988, Vol. 24, No 3. ISBN: 0412-1961
- [16] R. W. Cahn. 1991. Binary Alloy Phase Diagrams—Second edition. T. B. Massalski, Editor-in-Chief. ASM International, Materials Park, Ohio, USA. December 1990. ISBN: 978-0-87170-403-0, DOI:10.1002/adma.19910031215.
- [17] Z. L. Zheng, F. Ye. 2011. Formation of columnar-grained structures in directionally solidified Fe-6.5wt%Si alloy. *Intermetallics*, February 2011, Vol. 19, Issue 2. ISSN: 0966-9795, DOI:10.1016/j.intermet.2010.08.022.